Air-Gap Power Vector Based Sensorless Method for DFIG Control without Flux Estimator

G. D. Marques, *Member, IEEE*, and D. M. Sousa, *Member, IEEE*

***Abstract*— A sensorless method for the direct estimation of the slip position of the wound-rotor induction machine is introduced, discussed and experimentally validated in this paper. The slip position is necessary for the implementation of control by flux orientation. The method proposed is based on the phase comparison of an estimated air-gap power vector and the measured rotor currents in a common reference frame. The proposed method can be implemented in the rotor or in the field reference frames with a hysteresis or with a PI controller. The method is sensitive to the stator no load active and reactive power, but this dependence is not very important. Simulation and experimental results show that the method is appropriate for the vector control of the doubly fed induction machine. Unlike other methods, this method gives acceptable results when the load is small. In addition it does not need a flux estimator for the implementation of flux orientation.**

***Index Terms*—DFIG, Induction generator, Sensorless.**

I. Introduction

The Doubly-Fed Induction Generator (DFIG) is very attractive for Adjustable Speed-Constant Frequency (ASCF) generators with limited speed range. In this system, the stator circuits of the wound induction machine are directly connected to the AC mains and the rotor circuits are supplied by one back-to-back pulsewidth modulated (PWM) converter. This provides flexibility of operation in sub-synchronous and super-synchronous speeds both in the generating and motoring modes.

The rating of the power converter is determined by the operating speed range, normally limited to one third below and above the synchronous speed [1], and it is lower than the machine rating. This is a major advantage of the system.

Manuscript received June 8, 2010. Accepted for publication December 29, 2010. This work was supported in part by the Center for Innovation in Electrical and Energy Engineering, CIEEE.

G. D. Marques and D. M. Sousa are with Technical University of Lisbon, Instituto Superior Técnico, Department of Electrical and Computer Engineering (phone: 351-218417431; e-mail: gil.marques@ist.utl.pt and duarte.sousa@ist.utl.pt).

The major objective of the DFIG control is to obtain decoupling in the active and reactive power chains. The conventional approach is the implementation of stator flux orientation. In this case, the active and reactive powers are controlled by the quadrature and by the direct rotor current components respectively. The performance of the system depends on the detection of the stator flux reference frame position and the detection of the rotor position, derived from a position encoder or from a sensorless detection algorithm as considered in this paper.

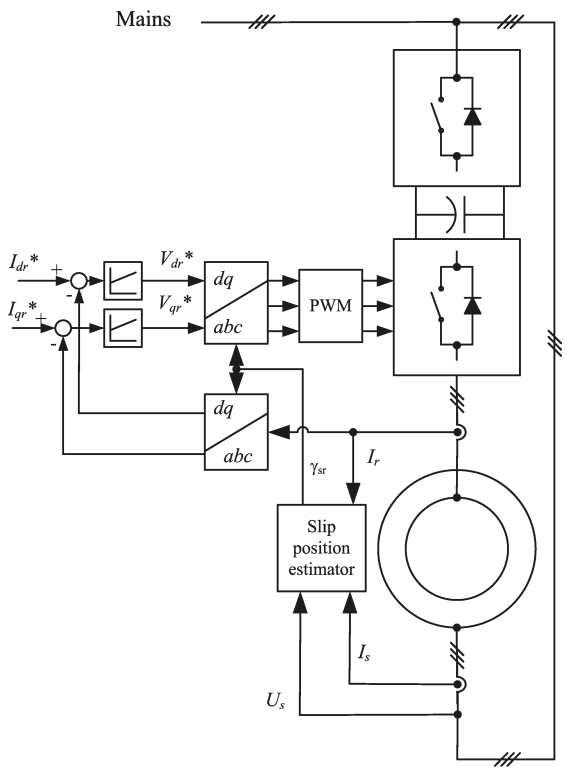

Fig. 1. Block diagram for the implementation of field orientation.

Since the power converter is connected to the rotor, it is mandatory to know the angular rotor position to implement the proposed control. Although the control is implemented in the field reference frame, it is necessary to implement a reference frame transformation from the field to the rotor reference frame. In fact, the necessary variable to allow decoupling is the difference of the stator flux position and the rotor mechanical position, which is the slip position.

There are major challenges in designing a position sensorless for a doubly-fed wound rotor induction machine. The algorithm should be stable and work well at any speed of the working range including near the synchronous speed. The rotor detection position system should be able to start on the fly, that is, it should converge on the correct position after some period of time, when the system starts working, without the knowledge of any initial condition [5].

Various sensorless-control techniques have been developed for DFIG [2] - [17].

The sensorless methods presented in [2]-[7] are open loop and based on the estimation of the rotor currents. The rotor position is obtained using the comparison of the estimated and the measured rotor currents. In [8] a sensorless method that uses only the rotor voltages and currents was reported. The flux is obtained by the integration of the rotor back-electromotive force. Near the synchronous speed, the frequency of rotor voltages or currents is low resulting in a poor performance.

The sensorless methods presented in [9]-[17] are based on the Model Reference Adaptive System (MRAS) technique that, in this case, can be interpreted as a Vector Phase Locked Loop (PLL). Some are implemented on the rotor reference frame [9]-[12], others on the stator reference frame [13]-[14], and others in both reference frames [15]-[17]. The controller is a Proportional Integral (PI) controller [9]-[14] or a hysteresis controller [15]-[17].

The usual approach of sensorless control consists in detecting the rotor and the stator flux positions and therefore uses the difference of these two values, to make the transformations shown in Fig. 1.

Some methods use an estimation of the stator flux to obtain the estimation for the rotor position [7]-[17]. This stator flux estimator can be implemented integrating the voltage applied to the stator, corrected by the stator resistive voltage drop which is normally very small. In the practical implementation, it is necessary to use mechanisms to correct the influence of the sensor offsets and initial conditions. When there are voltage dips, the stator flux starts to oscillate at the mains frequency.

This paper presents a different approach for a sensorless algorithm to detect directly the slip position without the estimation of the flux and the rotor position. It uses the measured rotor current and an estimation of the active and reactive power transferred across the air gap. Sometimes, the stator flux, multiplied by the slip frequency, is used in the quadrature current control as the feed forward element for decoupling [1], [13]. This can be avoided if for the synthesis of the PI current control the symmetry criterion is adopted [18]. The method proposed can be implemented in the field or in the rotor reference frames.

In a previous conference paper [16], an early version of the proposed control algorithm was discussed and in part experimentally tested. This paper presents the method, its stability and sensibility analysis, simulation and experimental results and shows that it is appropriate for DFIG control allowing decoupling of stator active and reactive powers.

To simplify the exposition of the algorithm in this text and of the implementation in the laboratory, *per unit* values are used.

The paper is organized as follows: In section II the proposed algorithm is described. Section III presents simulation results based on a tool constructed in the MatLab/Simulink environment. Sections IV and V presents the stability and sensibility analysis respectively. Section VI presents some experimental results obtained with a prototype constructed using a low-price fixed-point DSP. Section VII presents the conclusions and section VIII presents the nomenclature.

II. Description of the Method

A. Mathematical Model.

The method analyzed in this paper is derived from the classical model of the induction machine. Considering the voltage equations of the stator circuits, on the stator reference frame, in motor convention and *per unit* values, using the time in seconds:

$$u_{\alpha s} = r_s i_{\alpha s} + \frac{1}{\omega_s}\frac{d\psi_{\alpha s}}{dt}$$
$$u_{\beta s} = r_s i_{\beta s} + \frac{1}{\omega_s}\frac{d\psi_{\beta s}}{dt} \quad (1)$$

The stator flux vector $\boldsymbol{\psi_s} = (\psi_{\alpha s}, \psi_{\beta s})$ can be obtained using the classic voltage estimator based on the previous equation:

$$\psi_{\alpha s} = \omega_s \int (u_{\alpha s} - r_s i_{\alpha s})dt$$
$$\psi_{\beta s} = \omega_s \int (u_{\beta s} - r_s i_{\beta s})dt \quad (2)$$

The practical implementation of the flux estimator described in (2) depends on the initial conditions elimination and suffers also from the flux-integrator's drift problem. Other flux estimators can be also used [20]. For the implementation of stator flux orientation of DFIG, the actual position of the vector $\boldsymbol{\psi_s}$ is necessary. It is also necessary to know the mechanical position of the rotor. Therefore, only the difference $\gamma_{sr} = \gamma_s - \gamma_m$ is used to control the system.

Due to its simplicity for describing the proposed method, the Γ representation of the Induction Machine model will be used. This is well known from the classical literature and is presented in Fig. 2 for steady state. For transient regime the parameters and variables are defined in the same way.

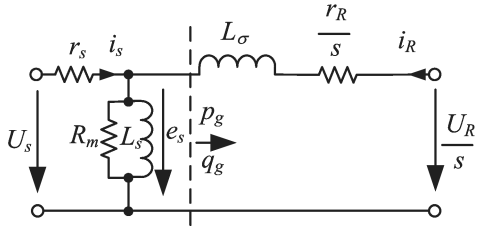

Fig. 2. Equivalent Γ circuit of the induction machine in steady state.

Where:

$$i_R = \frac{M}{L_s} i_r$$
$$U_R = \frac{L_s}{M} U_r \qquad \psi_R = \frac{L_s}{M} \psi_r \tag{3}$$
$$r_R = \left(\frac{L_s}{M}\right)^2 r_r$$

Defining the electromotive force vector $\boldsymbol{e_s}$ = ($e_{\alpha s}$, $e_{\beta s}$) as (Fig. 2 and Fig. 3):

$$e_{\alpha s} = \frac{1}{\omega_s}\frac{d\psi_{\alpha s}}{dt} = u_{\alpha s} - r_s i_{\alpha s}$$
$$e_{\beta s} = \frac{1}{\omega_s}\frac{d\psi_{\beta s}}{dt} = u_{\beta s} - r_s i_{\beta s} \tag{4}$$

The active and reactive powers transferred across the air gap are given by:

$$p_g = e_{\alpha s} i_{\alpha s} + e_{\beta s} i_{\beta s} - p_m$$
$$q_g = e_{\beta s} i_{\alpha s} - e_{\alpha s} i_{\beta s} - q_m \tag{5}$$

where p_m and q_m represents the active and reactive powers consumed at no load represented in Fig 2 by the R_m and L_s parameters. Being p_m and q_m functions of the electromotive force, in this paper they are assumed to be functions of the square of the electromotive force and are adjusted according to

$$p_m = \frac{e_{\alpha s}^2 + e_{\beta s}^2}{R_m} \qquad q_m = \frac{e_{\alpha s}^2 + e_{\beta s}^2}{L_s}. \tag{6}$$

In field coordinates, the active and reactive powers that reach the rotor from the air gap can be given also by:

$$p_g = -\left(e_{ds} i_{dR} + e_{qs} i_{qR}\right) = -|\boldsymbol{e_s}| i_{qR}$$
$$q_g = -\left(e_{qs} i_{dR} - e_{ds} i_{qR}\right) = -|\boldsymbol{e_s}| i_{dR} \tag{7}$$

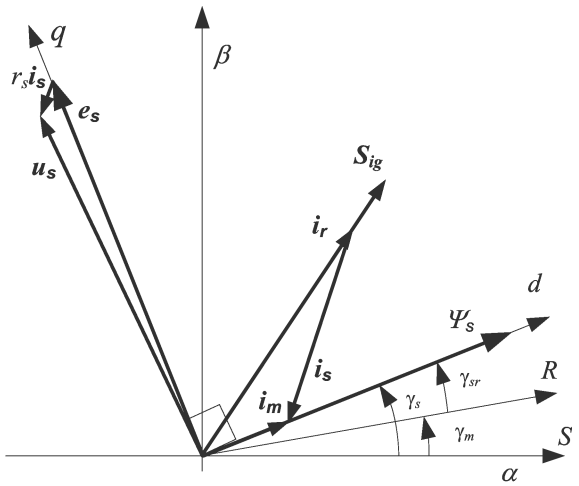

Fig. 3. Vector definitions in the implementation of stator-flux orientation.

Considering Fig. 3, since the electromotive force vector $\boldsymbol{e_s}$ is in quadrature with the stator flux vector, (7) can be used to obtain an expression for the estimated rotor currents on stator flux reference frame. The rotor currents will be estimated with the aid of active and reactive powers transferred across the air gap.

$$\hat{i}_{dR} = -\frac{q_g}{|\mathbf{e_s}|} \qquad \hat{i}_{qR} = -\frac{p_g}{|\mathbf{e_s}|} \tag{8}$$

These quantities are estimated on the flux reference frame. The measured rotor currents and the estimated rotor currents (8) can be used for the estimation of the rotor position as in [10], [12], [13]-[15]. In this paper the air-gap power vector

$$\boldsymbol{S_{ig}} = (-q_g, -p_g) \tag{9}$$

is used for the estimation of the slip position. In this way, the flux estimator is not necessary.

B. Description of the Estimator.

The detection of the rotor position can be performed using the mechanism shown in Fig. 4.

1) System implemented in the rotor reference frame.

The slip position, in the proposed method, is obtained from the output of the integrator, as show in Fig. 4. This integrator transforms the output of the hysteresis comparator into the slip position. Analyzing Fig. 4a, it is clear that the hysteresis comparator is fed by the cross product of the rotor measured current and the estimated air-gap power vector transformed to the rotor reference frame. Those two quantities should have the same frequency and phase. If so, the angle of transformation, that is, the slip position angle will be the correct value.

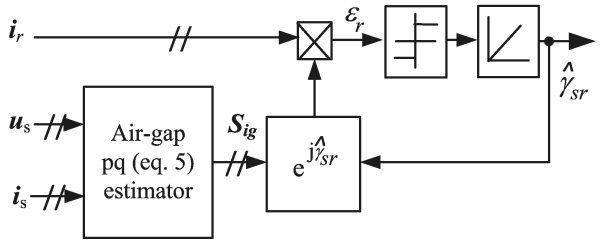

a) Rotor reference frame implementation.

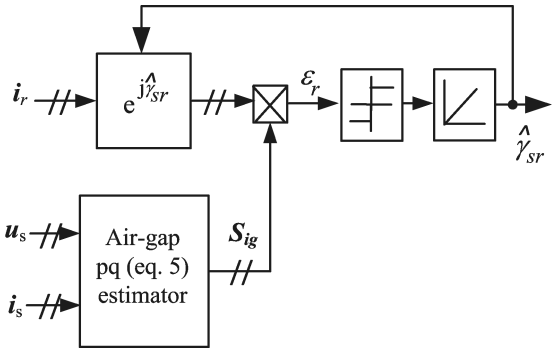

b) Field reference frame implementation.

Fig. 4. Rotor position estimator structure.

The transformation of the power vector $\boldsymbol{S_{ig}}$ is defined by:

$$\begin{bmatrix} S_{igx}^{r} \\ S_{igy}^{r} \end{bmatrix} = \begin{bmatrix} \cos\gamma_{sr} & -\sin\gamma_{sr} \\ \sin\gamma_{sr} & \cos\gamma_{sr} \end{bmatrix} \begin{bmatrix} -q_g \\ -p_g \end{bmatrix} \tag{10}$$

System implemented in the field reference frame.

In this case the measured rotor currents should be transformed to the field coordinates, Fig. 4b.

The detection principle is similar to the previous case, with similar results.

C. Implementation of the Hysteresis Controller.

So far, the methods presented in the literature [7] - [10] and [14]-[16] uses the cross product of an estimated rotor current with a measured rotor current, thus:

$$\varepsilon_r = \hat{\boldsymbol{i}}_r \times \boldsymbol{i}_r \tag{11}$$

In this paper, a similar reasoning is used. To avoid the division in (8), since the vector $\boldsymbol{S_{ig}}$ is collinear with the estimated rotor current, the active and reactive powers are used. So:

$$\varepsilon_r = \boldsymbol{S_{ig}} \times \boldsymbol{i_r} = q_g \cdot i_{dr} - p_g \cdot i_{qr} \tag{12}$$

The error ε_r is the input of a hysteresis controller that switches on or off when it is positive or negative respectively. The average value of this output coincides with the slip speed of the machine in steady state. In both limits, where only one output is used, the two outputs of this controller lead to the speed range of this system. In order to establish this speed range at $[0, 2\omega_s]$, the output of the hysteresis controller is set at $[-\omega_s, \omega_s]$. In a hysteresis controller there is also the need of determining its width, a *delta* parameter. In this case, a *delta*=0 can be used, because it is a sampled system and the estimation process does not give rise to chattering.

A PI controller can also be used. In this case the PI parameters should be determined. Normally, the symmetry criterion is used [21] leading to PI parameters that are function of the rotor current and of the electromotive force amplitude. The bandwidth of the control system should be high enough to allow synchronization. The hysteresis controller presents higher bandwidth and was preferred in this paper.

The method works well in the two reference frames described. No difference was found in simulation and in the laboratory.

The major advantages of this method are that it is not necessary to estimate rotor or stator fluxes, (since it uses measured voltages and currents), it is not necessary to perform any integration in open loop, and when a hysteresis controller is used, the synthesis of their parameters depends only on the required speed range where the system is working.

III. Simulation Results

A MatLab/Simulink program was constructed to determine the behavior of the proposed estimator included in the control system of the DFIG. To evaluate the performance of the method for large machines, parameters of a 2 MW wound rotor machine were used in simulations. This program will be also used for the sensitivity analysis.

A simulation result for N = 1.2 p.u. is shown in Fig. 5. The slip position decreases in time as expected. The d-q rotor currents as well the active and reactive powers P_e and Q_e are shown. The starting on the fly is also visible since the initial estimated and real slip positions are different.

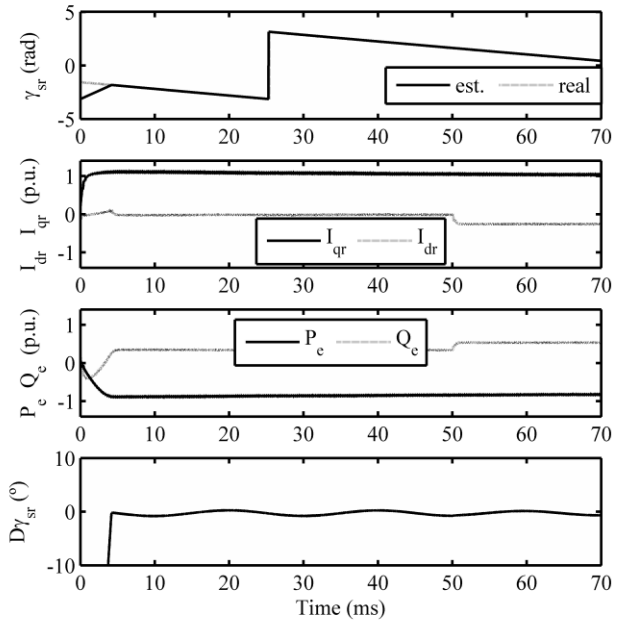

Fig. 5. Simulation results for rated current and starting on the fly.

The variable $D\gamma_{sr}$ measures the difference, in degrees, between the estimated slip position and the slip position that would be measured if the classical method was applied. In this last case, the slip position is determined by the difference between the stator vector flux position angle γ_s and the rotor position γ_m. So, considering Fig. 3:

$$D\gamma_{sr} = \hat{\gamma}_{sr} - (\gamma_s - \gamma_m) \tag{13}$$

According to the simulation result of Fig. 5, this variable is very small when the parameters of the machine are accurately determined.

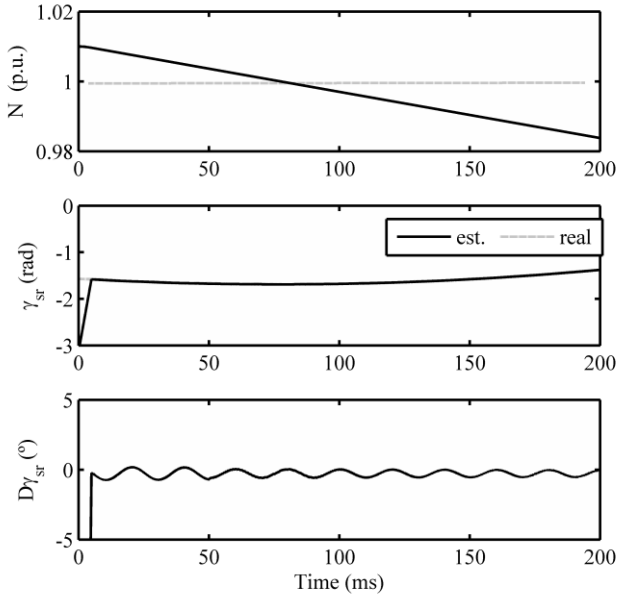

Fig. 6. Simulation results for crossing the synchronous speed.

The transient to obtain the correct position is clearly shown and lasts about 5 ms. After the transient, the system determines the real slip position without significant errors.

In Fig. 6 the results obtained when the DFIG is crossing the synchronous speed are shown. An almost constant slip position is obtained as expected.

IV. Stability Analysis

The stability analysis can be performed using a small-signal model as usual [10], [12] and the stability theory of sliding mode systems [19].

The error ε_r is defined as the cross product between the air-gap power vector and the rotor current vector, that is:

$$\varepsilon_r = \boldsymbol{S}_{ig} \times \boldsymbol{i}_r = |e_s||i_R||i_r|\sin(\delta) = \frac{M}{L_s}|e_s||i_r|^2 \sin(\delta) \qquad (14))$$

In steady state, the angle between $\boldsymbol{S}_{ig}$ and $\boldsymbol{i}_r$, i.e. δ, is null. This means that the rotor vector and the power vector rotated of $\hat{\gamma}_{sr}$ will be in phase (see Fig. 4a). When there is a positive perturbation $\Delta\hat{\gamma}_{sr}$ in the estimation angle, the power vector will undergo greater rotation and consequently it will be in advance relative to the rotor current vector. The cross product will be negative and:

$$\varepsilon_r = -\frac{M}{L_s}|e_s||i_r|^2 \sin(\Delta\hat{\gamma}_{sr}) \qquad (15)$$

For small perturbations, the classical approximation for sinus ($\sin \xi \approx \xi$, in rad) can be assumed giving:

$$\varepsilon_r = -\frac{M}{L_s}|e_s||i_r|^2 \Delta\hat{\gamma}_{sr} \qquad (16)$$

The small signal model, in p.u., Fig. 7, can be obtained when Fig. 4 is taken into consideration. The natural sampling of the system is represented by the sample and hold element, Fig.7.

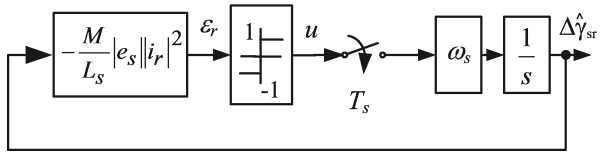

Fig. 7. Small-signal model for MRAS stability study.

According to the stability condition of sliding mode systems, the stability is guaranteed if the product of the error ε_r by its derivative is always negative [19]. The fulfillment of this inequality ensures the convergence of the system state trajectories to the sliding surface ε_r =0.

From the model, it can be concluded using *p.u.* values:

$$\frac{d\varepsilon_r}{dt} = -\frac{M}{L_s}|e_s||i_r|^2 \omega_s u \qquad (17)$$

Analyzing the two possible conditions:

$$\begin{aligned} &\varepsilon_r < 0 \quad \rightarrow \quad u = -1 \quad \rightarrow \frac{d\varepsilon_r}{dt} = \frac{M}{L_s}|e_s||i_r|^2 \omega_s > 0 \\ &\varepsilon_r > 0 \quad \rightarrow \quad u = 1 \quad \rightarrow \frac{d\varepsilon_r}{dt} = -\frac{M}{L_s}|e_s||i_r|^2 \omega_s < 0 \end{aligned} \qquad (18)$$

For the proposed solution, the stability condition mentioned above is verified.

V. Sensibility Analysis

A. Sensibility to Induction Machine Parameters.

Since the method presented is based on the phase comparison of the air gap power vector and the measured rotor current, the sensibility to parameter variations can be studied with the formulas (4), (5) and (6) used to obtain the active and reactive powers that crosses the air gap. The system is dependent on the stator resistance, and on the active and reactive powers at no load. The resistive voltage drop is small when compared with the applied voltage on the stator. The sensibility to this parameter is low. The most important parameters are the iron losses and the reactive power at no load. The first parameter, because it is very small, is practically not important. This no-load active power value suffers a discontinuity when the synchronous speed is crossed: Its decrease is double that of the rotor hysteresis losses. This is only visible when there is very low load and a very small $D\gamma_{sr}$ is required. The reactive power at no load is dependent on the stator self-inductance L_s. To avoid errors due to the voltage

level variations, this parameter is computed at each control step using (6).

The sensitivity to the stator inductance parameter is illustrated in Fig. 8 where a simulation result with 20% error in the self inductance parameter is shown. In this case, an error in the estimation value is obtained as can be observed. It depends on the parameter error and on the rotor current level. Table 1 shows the results obtained for several rotor currents and inductance values. These values were obtained considering I_d = 0, i.e., all the magnetizing current is fed from the stator. Similar results are presented in Table 2 when all the magnetizing current is supplied from the rotor. It can be concluded that, when higher values of I_d are considered, the error decreases considerably when I_q is small, but remains for higher values of I_q. The error is practically not dependent on the speed neither on the acceleration. As can be observed, when the inductance used in the calculations is smaller than the real value L_s^*, the error is positive, and when greater, it is negative. This dependence is similar when other methods are used [12]-[17].

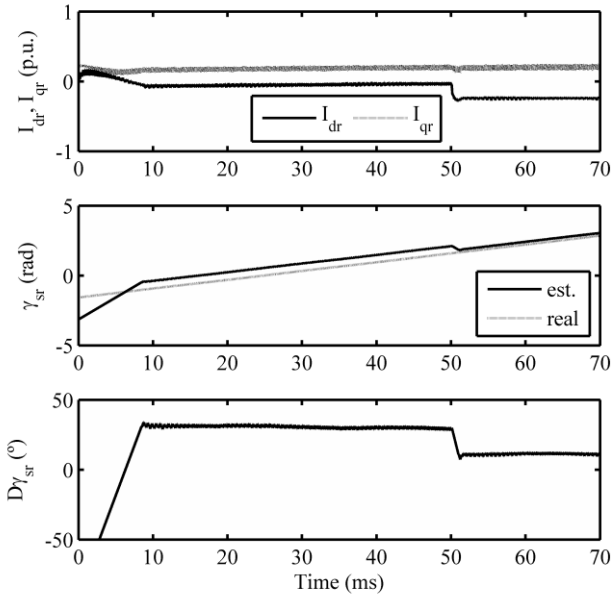

Fig. 8. Simulation result using a lower stator inductance parameter.

TABLE 1
Simulation Results in Degrees for the Rotor Estimation Error Considering N=1.0 p.u., I_{dr}=0

I_{qr} (p.u.)	$L_S=0.8L_S^*$	$L_S=0.9L_S^*$	$L_S=1.1L_S^*$	$L_S=1.2L_S^*$
1	6	3	-2.5	-4
0.5	12	5	-4.6	-8.2
0.25	25	10.5	-9	-15

TABLE 2
Simulation Results in Degrees for the Rotor Estimation Error Considering N=1.0 p.u., I_{dr}=0.32 p.u.

I_{qr} (p.u.)	$L_S=0.8L_S^*$	$L_S=0.9L_S^*$	$L_S=1.1L_S^*$	$L_S=1.2L_S^*$
1	5.1	2.1	-2.2	-4
0.5	8.1	3.4	-3.3	-5.8
0.25	8.6	3.6	-3.5	-6.2

The parameters p_m and q_m can easily be obtained in a no load test. This can easily be done with null rotor current and using the system to measure the active and reactive powers absorbed on the stator. The copper losses should be taken into account.

B. Sensibility to Stator Voltage Sensor Offsets.

The response to the system on the stator voltage sensor offsets is illustrated in Fig. 9, where a 5% offset on the sensor of phase 3 is considered. There are steps on the *d-q* rotor reference currents as can be seen in Fig 9. The P_e and Q_e variables are shown. It can be concluded that the system has an acceptable response. To evaluate the error, in this case, stator fluxes without the influence on the voltage offset are used because the removal of the offsets when calculating the flux is considered absolutely essential. This can be done using an automatic offset removal as will be described in the next section.

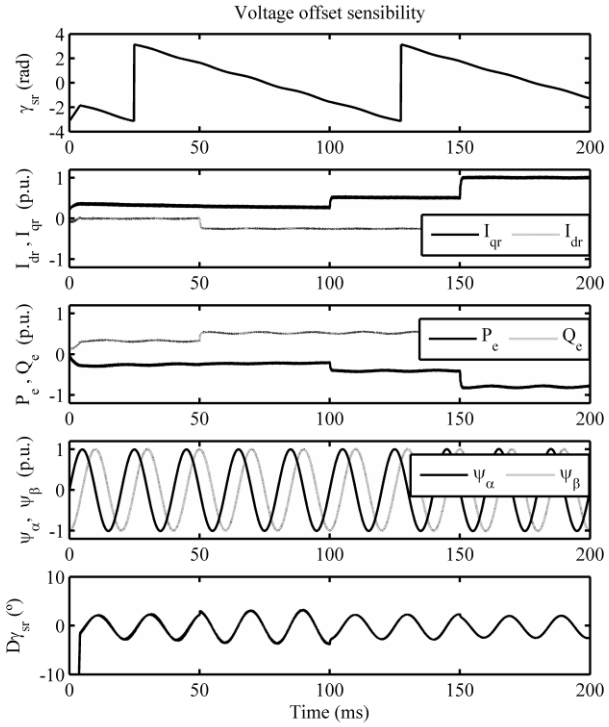

Fig. 9. Sensibility to stator voltage sensor offsets (N=1.2.p.u.).

C. Sensibility to Stator Current Sensors Offsets.

The sensibility to the stator current sensors offset was studied in the same way as for the stator voltages. The system works also adequately.

D. Sensibility to Rotor Current Sensor Offsets.

Because the method uses a phase comparison between the measured rotor current vector and the air-gap power vector, an offset on the rotor current sensors affects the estimation. In this case, when the system is working at the synchronous speed, the rotor currents are DC variables, and so, no automatic offset elimination can be used. Fig. 10, with steps on the reference currents, shows the response of the system when an offset on

the rotor current sensor is considered. This offset gives rise to an oscillation at slip frequency on the slip position angle as well in the $D\gamma_{sr}$ variable. This is particularly visible at low rotor currents.

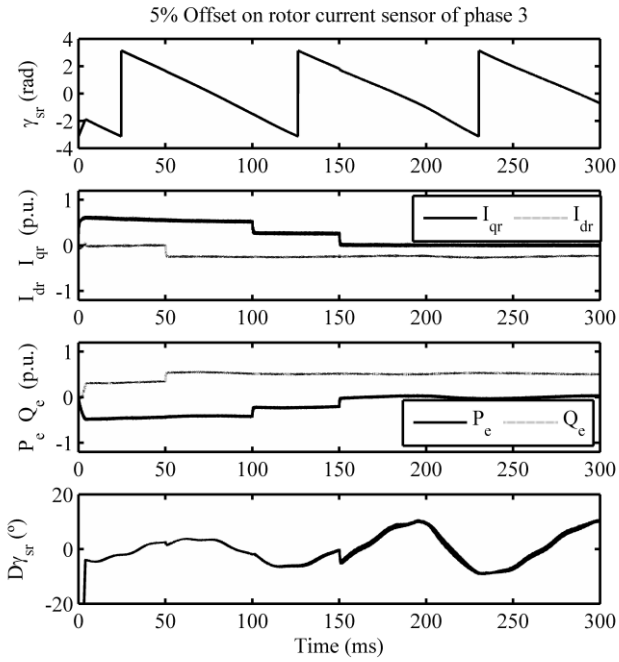

Fig. 10. Sensibility to rotor current sensor offsets (N=1.2.p.u.).

This offset can be eliminated manually, reading the rotor current output sensor values when the rotor currents are null.

VI. Experimental Results

This section presents some experimental results obtained in a prototype using a 3.2-kW wound induction machine driven by a DC machine. This DC machine can be used to emulate a wind turbine or another prime mover. It can deliver or absorb mechanical power from the rotor. Current transducers are used to measure the stator and rotor currents. The stator voltages are measured by two voltage transducers. The estimation and control algorithms are implemented in a Microchip dsPIC30F4011. To obtain experimental results in real time, four PWM output channels with simple RC filters were used. The actual rotor position is also measured using an encoder with a 4096 step resolution and the Quadrature Encoder Interface (QEI) module of this dsPIC. Because a 2-pole pair machine was used, the electrical position resolution decreases to 2048. This encoder was used only for comparison purposes and was calibrated in order to align its zero point with the zero position of the machine leading to an error smaller than 1 degree. The sampling frequency used was 10 kHz.

A. Practical Issues.

Information about the stator flux is not necessary to implement this method. However, to compare the estimated slip position with the one obtained with the classical method, it is necessary to implement a stator flux estimator. In practice, for the evaluation of the flux, it is necessary to eliminate the effect of the stator A/D converter offsets. This was performed using an automatic ADC offset elimination. This was implemented maintaining a running average of the ADC offset that is subtracted from the ADC output value before scaling. The offset is accumulated as a 32-bit signed integer and is used to correct the raw ADC. This procedure is equivalent to using a high pass filter with a time constant of 6.5 s.

The automatic offset elimination was implemented only on the stator voltage and current measurements. It was not used on the rotor current ADC conversion because, at synchronous speed, these variables are of zero frequency, and this system will eliminate not only the offset, but also the actual measurement. In this case a manual offset elimination was implemented.

The automatic offset elimination is much more important when a flux estimator is used because this is implemented using the integration of the stator voltages. Offset values in this case are not allowed.

To evaluate the estimated rotor position a flux estimator was used as was described in [17]. It uses a low pass filter and a phase corrector in order to have $\pi/2$ phase difference between the resulting flux and the electromotive force.

B. Results in Steady State.

Figures 11-13 show the behavior of the system in steady state at 3 different speeds when I_{dr}=0 and I_{qr}=-0.5 p.u.. These figures show the estimated slip position obtained, the α component of the stator flux that gives $\cos(\gamma_s)$, the α component of the rotor current and $D\gamma_{sr}$.

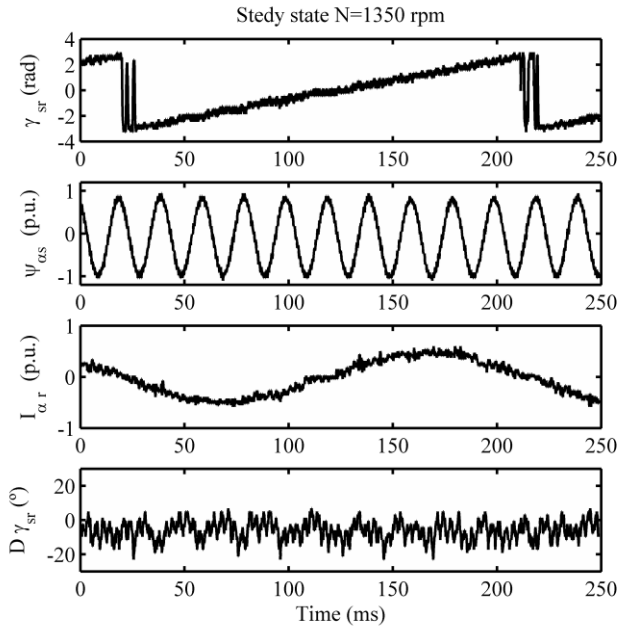

Fig. 11. Performance in steady state below the synchronous speed.

The slip position obtained behaves as expected. It increases, and decreases in time below, and above the synchronous speed respectively. At synchronous speed it is constant as also the rotor currents. The quantity $D\gamma_{sr}$ is presented in degrees to be

more visible and averages respectively -6.3º, -10.8º and -7.6º. These errors could be reduced if some adjustment was made on the L_s parameter. The L_s parameter used here was obtained using the classic no load test. On the transition of the slip position between $-\pi$ and π there is some oscillation. This is due to the fact that $-\pi$ and π represent the same position, and there is always some variation that is magnified in this case.

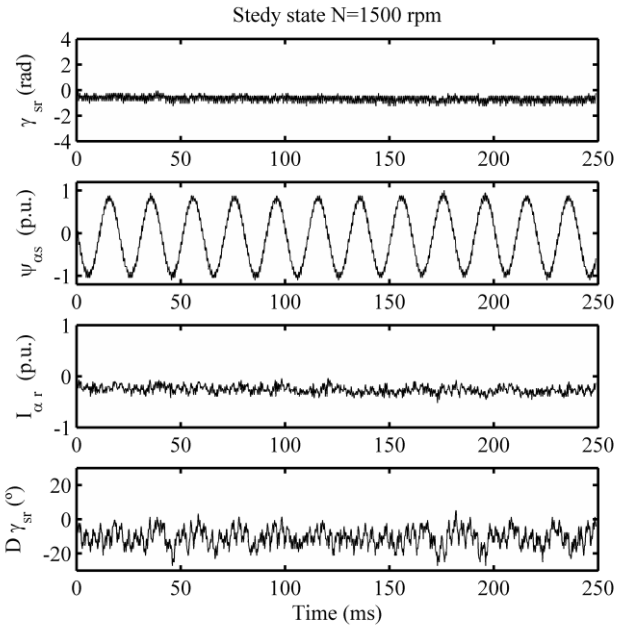

Fig. 12. Performance in steady state at the synchronous speed.

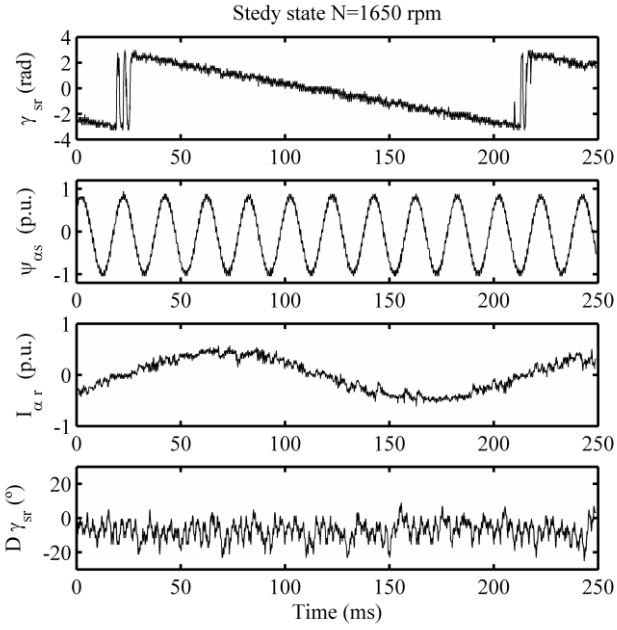

Fig. 13. Performance in steady state above the synchronous speed.

It was observed in the laboratory that the system works acceptably, but with errors, with loads as low as 3% of the rated rotor current.

C. *Starting on the Fly.*

An experimental result showing the result of starting on the fly is presented in Fig. 14. The starting estimated position is almost π (or -π). It decreases slowly when there is no current, but when the IGBTs are fired the rotor currents are flowing and the estimated position starts to converge on the correct position. This transient depends on the instant of switching on and can take different waveforms. This is done using a small amount of *d* and *q* rotor currents as can be seen.

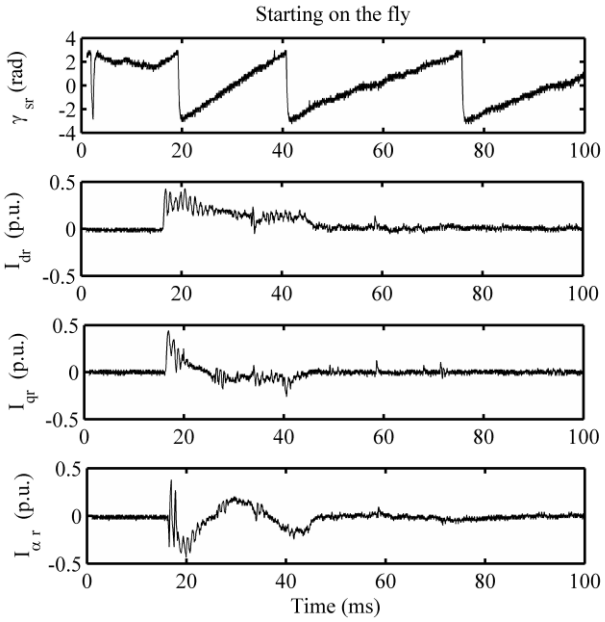

Fig. 14. Start on the fly transient.

D. *Response to Steps on the Reference Currents.*

The responses to steps on the direct and quadrature reference currents are presented in Fig. 15 and Fig. 16 respectively. As expected, there is a decoupling between the active and reactive control chains. When a step is applied on the direct rotor current, only the stator reactive power is changed. If a step is applied on the quadrature rotor current, only the active power changes. The proposed system shows itself to be appropriate for the active and reactive power control of the DFIG.

In Fig. 15, the reference I_{dr} was varied from -0.5 p.u. to 0.5 p.u. producing a negative step on the reactive power transferred on the stator. Even when I_{dr}=0.5 *p.u.*, the reactive power on the stator is still positive. This is due to the fact that, in this machine, the no load current is very important (0.62 p.u.).

In Fig. 16, the reference of I_{qr} was varied from 0 to 1 *p.u.*. The machine is working above the synchronous speed and produces a step on the active power as shown. In this case, the system starts working as a generator delivering active power to the network by the stator circuits.

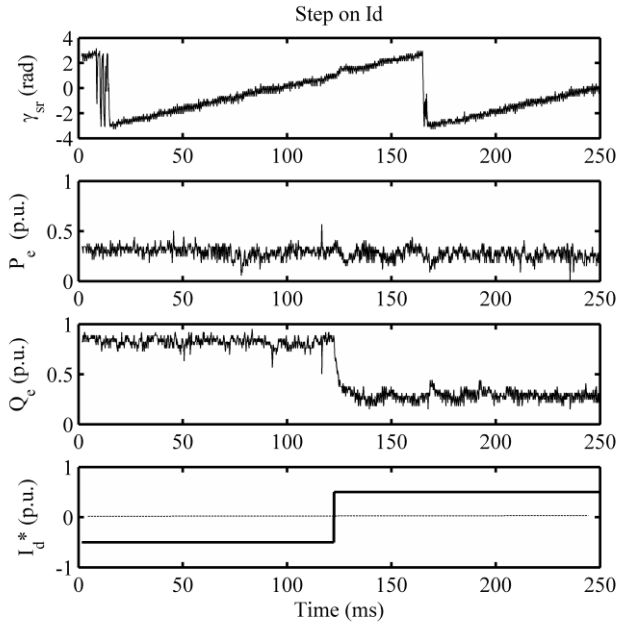

Fig. 15. Response to a step on the direct reference current.

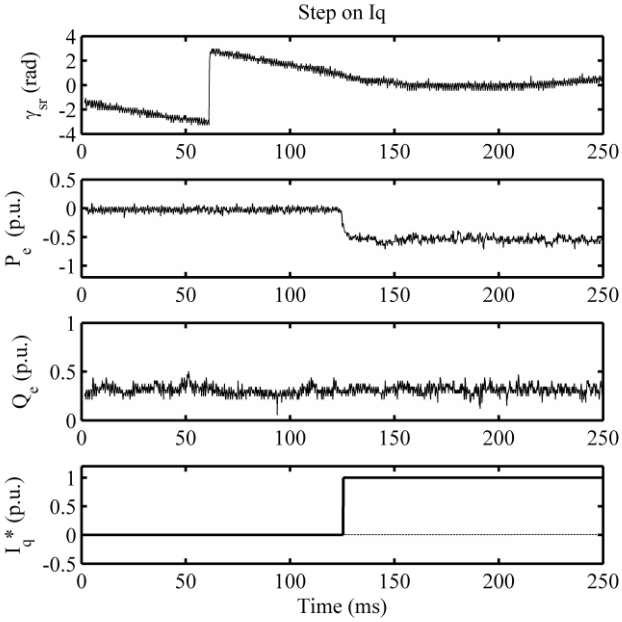

Fig. 16 Response to a step on the quadrature current.

E. Response at Variable Speed and Low Load.

The response at variable speed and low rotor current (I_{dr}=0, I_{qr}=-0.125 *p.u.*) is presented in Fig. 17.

The power electronic inverter, connected to the rotor, is switched on when I_{qr} changes, as can be seen in Fig. 17. The *d-q* rotor reference currents are constant. Because the load is low, the electromagnetic torque is sufficient to produce some acceleration. Near the instant *t*=1.4 *sec*, the system crosses the synchronous speed, as can be seen in Fig. 17. During the acceleration, the rotor *d-q* current components remain constant, as can be observed in Fig. 17.

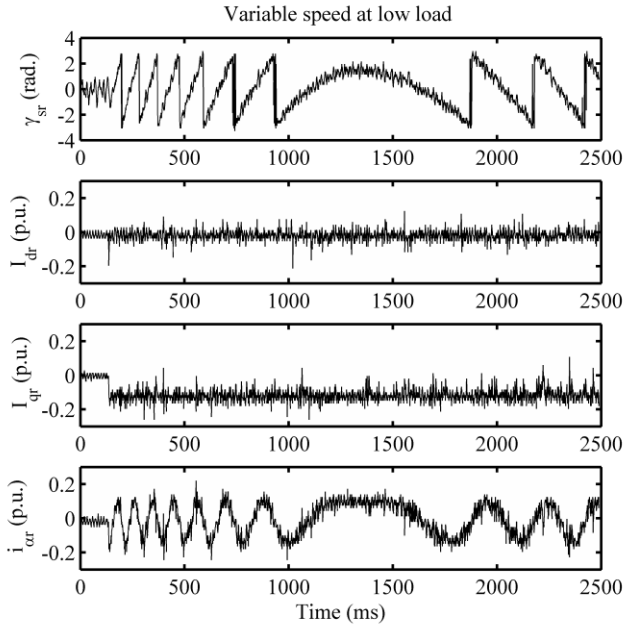

Fig. 17. Response at variable speed and low load.

VII. CONCLUSIONS

The paper presents a sensorless system for the estimation of the slip position of the DFIG. This variable is necessary for the implementation of field orientation. The proposed sensorless algorithm fulfills the requirements of the DFIG in general applications. Starting the system on the fly is easily accomplished. Although the performance of the system is dependent on the stator self-inductance L_s parameter, it was shown that the system works acceptably well with currents low as 3% of the rated rotor current.

VIII. NOMENCLATURE

General

ψ	Stator or rotor linkage flux.
L_s, M	Stator and mutual inductance.
r_s	Stator resistance.
i	Current.
u	Stator voltage.
e	Electromotive force.
N	Rotor speed.
P_e	Active power transferred on the stator minus the stator copper losses.
Q_e	Reactive power transferred on the stator.
p_g	Power transferred across the air gap.
q_g	Reactive power transferred across the air gap.
q_m	Reactive power consumed on the stator.
p_m	Stator iron losses.
R_m	Resistance for the representation of iron losses.
δ	Angle between $\mathbf{S_{ig}}$ and $\boldsymbol{i_r}$
γ_s	Position of the stator flux vector.
γ_m	Electrical position of the rotor.
γ_{sr}	Electrical slip position.
ε_r	Error.
ω_s	Electrical frequency of the ac mains.

$\boldsymbol{i_s}$ Stator current vector.
$\boldsymbol{i_r}$ Rotor current vector.
$\boldsymbol{u_s}$ Stator voltage vector.
$\boldsymbol{e_s}$ Electromotive force vector.
$\boldsymbol{\psi_s}$ Stator flux vector.
$\boldsymbol{S_{ig}}$ Air-gap power vector

Superscripts
^ Estimated value.
s, r Stator or rotor reference frame.
Subscripts
α, β Usual $\alpha\beta$ variables.
d, q Variables on a common moving reference frame.
s, r Stator or rotor quantities.
R Rotor variables or parameters of the Γ circuit.
g Airgap

The per-unit values are defined as usual, but using as base values, the peak of the rated values. Because the time is in seconds, the angular speed and frequency are in rad/sec. The synchronous speed is the base value for the rotor speed.

APPENDIX

Parameters of the DFIG

2-MW rated machine in the simulations

L_s=3.1 p.u., M=3 p.u., r_s=0.01 p.u, r_r=0.01 p.u. L_r=3.1 p.u.

Laboratory prototype

Induction Machine: stator 380 V, 8.1 A, rotor 110V, 19 A, 3.2-kW, four poles, 1400 rpm, L_s = 1.62 p.u., M = 1.17 p.u., r_s = 0.06 p.u.

REFERENCES

[1] R. Pena, J. C. Clare, and G. M. Asher, "Doubly fed induction generator using back-to-back PWM converters and its application to variable-speed wind-energy generation", *IEE Proc. Electr. Power Appl.*, vol. 143, pp. 231-241, May 1996.
[2] E. Bogalecka, "Power control of a double fed induction generator without speed or position sensor", *in Conf. Record EPE*, 1993, pt. 8, vol. 377, ch. 50, pp. 224-228.
[3] E. Bogalecka, Z. Krzeminski, "Sensorless Control of Double Fed Machine for Wind Power Generators" *EPE-PEMC 2002 Conf. Record*, Dubrovnik Cavat, 2002.
[4] Z. Krzeminski, A. Popenda, M. Melcer, P. Ladach, "Sensorless control system of double fed induction machine with predictive current controller" *EPE 2001 Conf. Record*, Graz, 2001.
[5] Rajib Datta, V. T. Rangaanathan, "A simple Position-Sensorless Algorithm for Rotor-Side Field-Oriented Control of Wound-Rotor Induction Machine" *IEEE Trans on Industrial Electronics*, vol. 48, No. 4, pp. 786-793, August 2001.
[6] L. Morel, H. Godfroid, A. Mirzaian, and J. M. Kaufmann, "Double-fed induction machine: converter optimization and field oriented control without position sensor", *IEE Proc., Electr. Power Appl.*, 1998, 145, (4), pp. 360-368.
[7] B. Hopfensperger, D.J.Atkinson and R. A. Lakin, "Stator-flux-oriented control of a doubly-fed induction machine with and without position encoder" *IEE Proc. Electr. Power Appl.*, vol. 147, No. 4, pp. 241-250, July 2000.
[8] Longya Xu, Wei Cheng, "Torque and Reactive Power Control of a Doubly Fed Induction Machine by Position Sensorless Scheme" *IEEE Trans. Industry Applications*, vol. 31, No. 3, pp. 363-642, May/June 1995.
[9] R. Cárdenas, R. Peña, G. Asher, J. Clare, J. Cartes, "MRAS Observer for Doubly Fed Induction Machines" *IEEE Trans on Energy Conversion*, vol. 19, No. 2, pp. 467-468, June 2004.
[10] R. Cárdenas, R. Peña, J. Proboste, G. Asher, J. Clare, "Rotor current based MRAS observer for doubly-fed induction machines" *Electronic Letters*, 10th, vol. 40, No. 12, June 2004.
[11] R. Cárdenas, R. Peña, J. Proboste, G. Asher, J. Clare, "Sensorless Control of a Doubly- Fed Induction Generator for Stand Alone Operation" *35th Annual IEEE Power Electronics Specialists Conference*, Aachen, Germany, 2004, pp. 3378-3383.
[12] Rubén Peña, Roberto Cárdenas, José Proboste, Greg Asher, and Jon Clare, "Sensorless Control of Doubly-Fed Induction Generators Using a Rotor-Current-Based MRAS Observer" *IEEE Trans. On Industrial Electronics*, vol. 55, NO. 1, pp. 330-339, January 2008.
[13] Baike Shen, Barkari Mwinywiwa, Yongzheng Zhang, Boon-Tek Ooi, "Sensorless Maximum Power Point Tracking of Wind by DFIG Using Rotor Position Phase Lock Loop (PLL)" *IEEE Transactions on Power Electronics*, vol. 24, No 24, pp. 942-951, April 2009.
[14] Bakari Mwinyiwiwa, Yongzheng Zhang, Baike Shen, Boon-Teck Ooi "Rotor Position Phase-Locked Loop for Decoupled *P-Q* Control of DFIG for Wind Power Generation" *IEEE Transactions on Energy Conversion*, vol. 24, no. 3, pp 758-765, September 2009.
[15] G. D. Marques, V. Fernão Pires, Sérgio Sousa, Duarte M. Sousa, "Evaluation of a DFIG Rotor Position-Sensorless Detector Based on a Hysteresis Controller" in *PowerEng Conference*, Costa da Caparica, Lisbon, 2009.
[16] G. D. Marques, Duarte M. Sousa, "A DFIG Sensorless Method for Direct Estimation of Slip Position", in Proceedings of IEEE SIBIRCON-2010, Irkutsk, Russia, July 11-15 2010, pp818-823.
[17] G. D. Marques, V. Fernão Pires, Sérgio Sousa, Duarte M. Sousa, "A DFIG Sensorless Rotor Position Detector Based on a Hysteresis Controller", *IEEE Trans. on Energy Conversion*, to be published.
[18] G. D. Marques, "Input-Output Linearization Based versus Classic PI Control of a three-phase AC/DC Converter" Industrial Electronics Conference, Porto, Portugal, November 3-5, 2009.
[19] Silva, Fernando A.; Pinto, S.; "Control Methods for Switching Power Converters", cap. 34, pp 935-998, in M. H. Rashid (Editor), Power Electronics Handbook, 2nd edition, Academic Press, Elsevier, pp 1172, ISBN 13:978-0-12-088479-7, ISBN 10:0-12-088479-8, USA, 2007.
[20] Daniel G. Forchetti, Guillermo O. Garcia, Maria Inés Valla, "Adaptative Observer for Sensorless Control of Stand-Alone Doubly Fed Induction Generator" *IEEE Transactions on Industrial Electronics*, vol. 56. No. 10, pp. 4174-4180, October 2009.
[21] Vikram Kaura, Vladimir Blasko, "Operation of a Phase Locked Loop System Under Distorted Utility Conditions" *IEEE Trans. Industry Applications*, vol. 33, no. 1, pp. 58-63, January/February 1997.

G. D. Marques (M'95) was born in Benedita, Portugal, on March 24, 1958. He received the Dipl. Ing., and Ph.D. degrees in electrical engineering from the Technical University of Lisbon, Lisbon, Portugal in 1981 and 1988, respectively.
Since 1981, he has been with the IST, Technical University of Lisbon, where he teaches Power Systems in the Department of Electrical and Computer Engineering. He is also a Researcher at the Center for Innovation in Electrical and Energy Engineering. His research interests include electrical machines, static power conversion, variable-speed drive and generator systems, harmonic compensation systems and distribution systems. Dr. Marques is a member of IEEE. He is an Associate Professor since 2000.

Duarte M. Sousa (M'09) was born in Viana do Castelo, Portugal, in 1970. He received the Dipl. Ing., M.S., and Ph.D. degrees in electrical and computer engineering from the Instituto Superior Técnico and the Technical University of Lisbon, Lisbon, Portugal, in 1993, 1996 and 2003, respectively.
In 1993 he joined the Technical University of Lisbon where he has been an Assistant Professor since 2003.